HEAT DISSIPATION PERFORMANCE OF GROOVED-TYPE AND COPPER FOAM-TYPE VAPOR CHAMBERS

by

Leiqing WANG, Donghui ZHANG**, *Yi CHEN, Lili SUN, and Jijing MAO

School of Power and Energy, Jiangsu University of Science and Technology, Zhenjiang, China

Original scientific paper
https://doi.org/10.2298/TSCI200821141W

Both grooved-type and copper foam-type vapor chambers are explored and investigated. The overall performance of vapor chamber depends on both axial and spread thermal resistance mutually. The copper foam-type vapor chambers achieved the lowest axial thermal resistance less than 0.2 K/W. The grooved-type sample presented the lowest spread thermal resistance, indicating better temperature uniformity. The visual experiment demonstrated that the evaporating surface of the copper-foam vapor chamber was dominated by the thin film evaporation mechanism at low charging ratio while dominated by the pulsed pool boiling mechanism at large charging ratio. For the grooved-type vapor chamber, the pool boiling mode was observed at any charging ratio.

Key words: *vapor chamber, heat dissipation, thermal resistance, copper foam, microgroove*

Introduction

Vapor chamber (VC) has been widely used in the field of electronic devices. The phase-change process in VC offers a possibility of high efficient heat transfer in mini space. The heat flux from the *hot spot* could be effectively dispersed uniformly across the VC.

The wick structure has a significant influence on the performance of VC. Excellent capillary structure can effectively enhance the liquid evaporation and provide the capillary pressure for liquid supply. Great progress [1, 2] has been made in the research of VC in recent years. Boukhanouf [3] compared the diffusion thermal resistance between the copper-powder-sintered VC and copper plate with the same size. The dimension of tested VC was 250 mm × 200 mm × 2 mm, and the heating area was 100 mm × 50 mm. The working fluid was water. The temperature difference of condensation surface was found less than 3 K from the infrared photography. The VC is only one fortieth in the diffusion resistance of the copper plate at the heat flux of 28 W/cm^2. In the paper [4] introduced a kind of multi-scale foamed copper wick made by the electroplating method, containing various sizes of pores in the range of 5~300 μm. Such a kind of wick structure can reduce the flow resistance and increase the liquid supply, compared with traditional capillary structure. In the paper [5] proposed Bi-layer compound capillary wicks to alleviate the contradiction between capillary force and flow resistance. This consideration has also been widely used up to now [6, 7]. In the paper [8] ap-

* Corresponding author, e-mail: dhzhang20@126.com

plied the sintered copper-powder pillars in the VC design to shorten the return path of condensate. Its heat transfer limit increased to about 380 W/cm^2. The lowest evaporation thermal resistance is 0.05 K/W. In the paper [9] studied heat transfer mechanism of coexistence of boiling and condensation in a limited space. Experimental observation shows that boiling and condensation process influences each other significantly, include the interaction between vapor bubbles and the condensate liquid film and liquid drops. The condensation heat transfer process plays a crucial role in the heat transfer ability of the confined phase change chamber. In the paper [10] found that the boiling mode was related by the charging rate. Too large charging rate resulted in pool boiling mode on the evaporation surface of VC while too small transform into the thin liquid film evaporation mode. It is easy to cause the evaporating surface to dry up.

The current research progress of VC lie in as follows. The thinner VC Zhaoshu *et al.* [11] puts forward high requirements for the manufacturing process, the compound capillary wicks [12, 13] are applied to alleviate the contradiction between the capillary force and flow resistance in VC, and the wick optimization and matching between the evaporating and condensing surface Xianbing [14].

In this paper, both the grooved-type and copper foam-type VC were studied. Both types of VC were investigated in detail, including axial and spread thermal resistance performance. The visual observation also was carried out to understand the operating mechanism in the VC.

Fabrication of vapor chambers

The VC, with size of 100 mm × 100 mm × 4.5 mm, is made by oxygen-free copper. The degassed and deionized water is used as the working medium. For two grooved-type samples, grooves along the radial direction serve as the wick structure, transporting the condensate to the evaporation area in the bottom. The chamber height is 1.8 mm, and the wall thickness of the upper and bottom plate is 1.2 mm and 1.5 mm, respectively. The rectangular grooves are processed by CNC machine. The structural parameters are depicted in tab. 1. The aspect ratio of the micro-groove is about 1.0~2.0. Both grooved-type samples have the same groove distribution in the condensation surface. The groove distribution of grooved-type 1 is shown in figs. 1(a) and 1(b). Evenly-distributed support columns in the upper plate ensure the structural strength of the VC after evacuation.

Table 1. Structural parameters of grooved vapor chambers

	Upper plate	Grooved I Bottom plate	Grooved II Bottom plate
Total thickness	3	1.5	1.5
Groove depth	0.5	0.5	0.5
Groove width	2	0.3	0.5
Number of grooves	18	48	60

Copper foam-type VC has the same size as the grooved-type ones. The SEM photos for both copper foam wicks are shown in fig. 2. Thin copper foam with a thickness of 0.6 mm is selected as the capillary wicks of evaporation and condensation surface. Its porosity is 65% and 85%, respectively. The main fabrication processes includes: cleaning, two-step sintering, leak detection, water-charging, vacuuming, and charge-tube sealing. Before sintering, carefully cleaning process is required to ensure no oxidative deterioration. Two-step sintering processes includes: in the first step, the copper foam wick and top (or bottom) plate are sintered together, then, the upper plate, bottom plate, and charging tube are integrated totally.

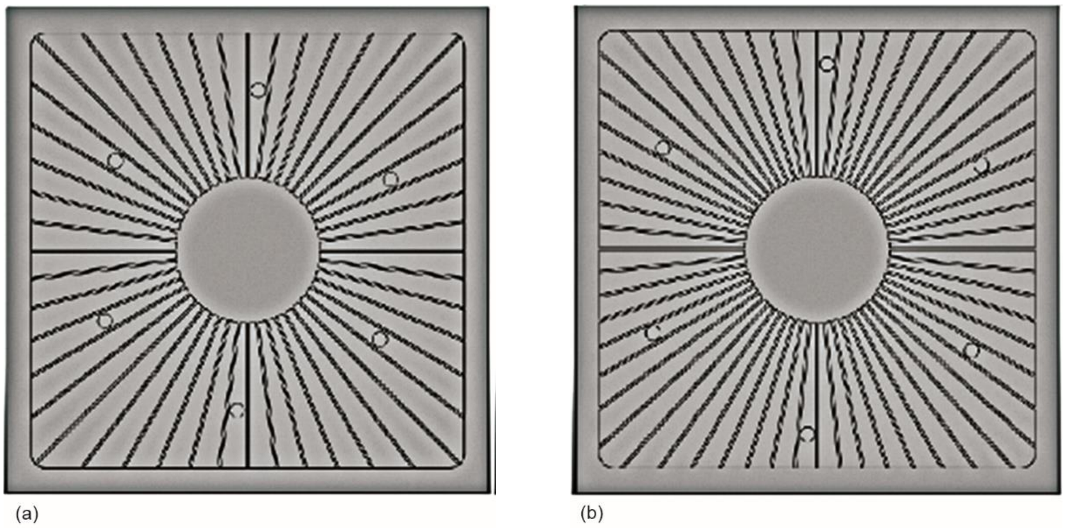

Figure 1. Radial grooved VC; (a) upper plate and (b) bottom plate

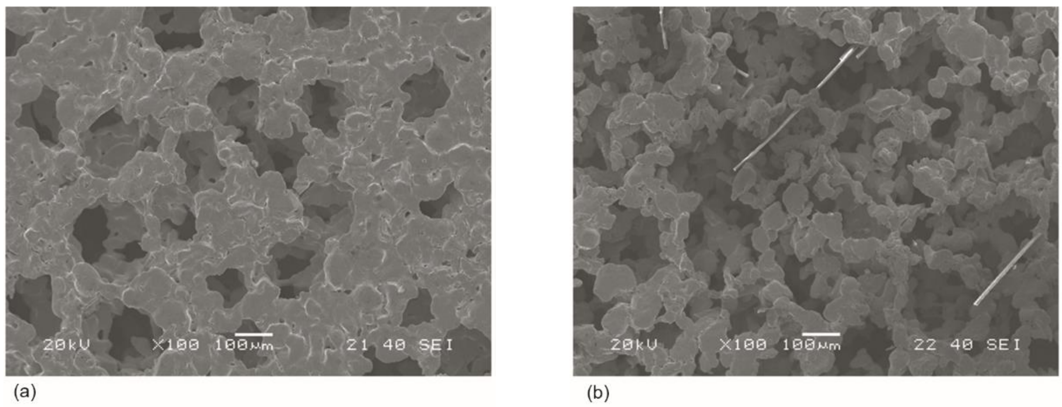

Figure 2. Micro-structure of both copper foam wicks with 100 times magnification; (a) copper foam I (porosity: 65%) and (b) copper foam II (porosity: 85%)

Experimental system

Performance measuring system

The performance measuring system consists of a pressure loader, the testing bench, electric heating source, water cooler, and data acquisition module. The measuring bench is shown in fig. 3. The pressure loader compresses the water cooler tightly on the VC to reduce in-between contact thermal resistance, and its spring dynamometer could indicate the magnitude of the ballast force. The water cooling method is applied to figure out the heat transfer rate dissipated by the condensing surface. The cooling water is supplied by a constant temperature water bath. The heat source is simulated by a heating copper block with four electric heating rods. The input power of heating rod, adjusted by the transformer, is measured by an

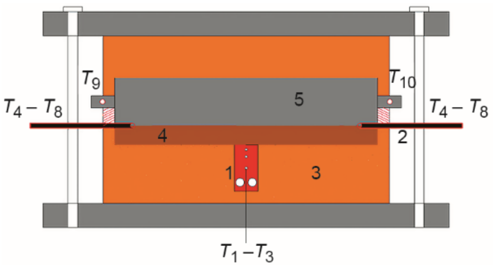

Figure 3. Testing Bench of VC;
1 – heater, 2 – thermocouple, 3 – insulation, 4 – vapor chamber, and 5 – cooler

intelligent electricity meter. A Bakelite jacket is wrapped around the heated copper block to ensure good thermal insulation. The heater area is 9 cm^2.

Five *K*-type thermocouples were inserted to measure the temperature distribution of condensation surface, and the other two *K*-type thermocouples to measure the copper block temperature along the heat flux direction. Two PT100 sensors were placed near the inlet and outlet of the water cooler to monitor fluid temperatures. All measured temperature data were real-time transformed by a data acquisition module and then recorded in computer by the MCJS software.

The calibrated *K*-type thermocouple have a temperature measurement uncertainty of ±0.5 K. The uncertainties of flow rate, input heat power are ±1%, and ±0.5%, respectively. The fluid temperatures of the cooler inlet and outlet are measured by two Pt100 with uncertainties of ±0.3 K. The relative uncertainty of both axis and spread thermal resistance is estimated below 5% by the standard error analysis method.

Visual system

The purpose of the visual experiment is to view the boiling process inside the VC, which is helpful to understand its operation mechanism. The visual system is displayed in fig. 4, chose copper foam-type 2 and grooved-type 2 as the study objects. The visualized VC is made of an upper cover plate, a stainless steel frame, and a copper-based bottom plate, as shown in fig. 5. The upper plate, processed from the transparent acrylic material, is combined with the bottom plate by bolts. The BNR O-ring seal ensure enough sealing between the upper and bottom plate. Two cuboid water jackets are arranged on both sides of the bottom surface. Before packaging, the acrylic cover plate is coated with a hydrophilic film to reduce the interference of condensation droplets in observation. Evacuation and water-charging process are carried out in due order after packaging. The internal operation state of the VC was captured by the Olympus high-speed camera. The heater area in the center region is 2.25 cm^2 or 9 cm^2.

Figure 4. Experimental system for visualization

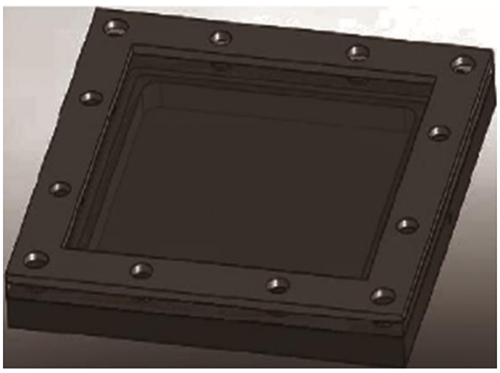

Figure 5. Visualized VC

Table 2. Charge ratio of each vapor chamber

	Grooved-type I	Grooved-type II	Copper foam-type I	Copper foam-type II
Charge quantity	1.9	1	6	5
Charge ratio	110.0	50.0	90.0	65.0

Results and discussion

Axial thermal resistance

In the experiment, the charging amount of each uniform temperature plate should be determined by the wick porosity (or volume percent of microgrooves), exhibited in tab. 2. The liquid-charging ratio of the samples ranges from 50% to 110%. The charging ratio is defined as the ratio of the charging liquid volume to the total pore volume of capillary wick. The performance test of each sample starts from 20 W and increases 10 W per time and each stabilization time is about 30 minutes. Once the thermal resistance will increase shapely, it indicates the heat transfer limit of tested VC.

The axial thermal resistance of the VC is defined [15]:

$$R = \frac{T_h - T_c}{Q} \tag{1}$$

where T_h is the center temperature of the bottom surface, T_c – the average temperature of the condensation surface, and Q – the input heating power.

The axial thermal resistance of each grooved-type sample is shown in fig. 6. From the overall trend, the grooved-type I presents lower thermal resistance than the grooved-type II. The thermal resistance of the grooved-type II ranges between 0.1~0.2 K/W. Both of samples bear the similar heat transfer limit, close to 120~130 W. Figure 7 shows the variation of thermal resistance of copper-foam samples with the heat flux. Both copper-foam samples have the similar performance in thermal resistance, especially in $Q \geq 60$ W. Overall, the copper foam-type VC presents slightly lower in thermal resistance than the grooved-type ones. The wick permeability and capillary pressure are referred in tab. 3 according to the structural parameters of samples. If the vacuum degree is the same, the performance of VC is mainly affected by the permeability, capillary pressure and charging rate. Largest capillary force ac-

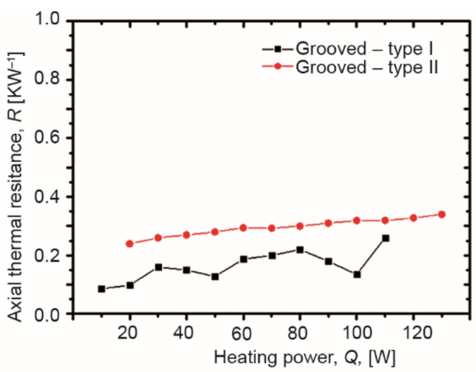

Figure 6. Axial thermal resistance of grooved-type VC

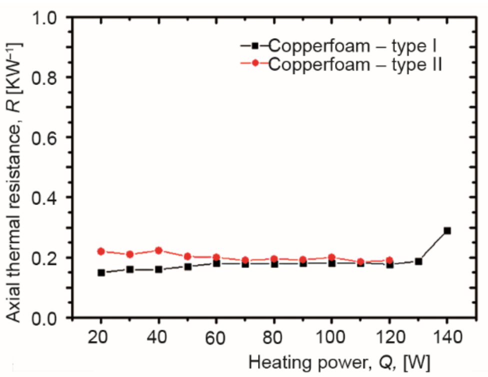

Figure 7. Axial thermal resistance of copper foam-type VC

Table 3. Parameters for all VC

	Porosity [%]	Hydraulic diameter [m]	Capillary pressure [Pa]	Permeability [m^{-2}]
Copper foam I	65	$1.2\cdot10^{-4}$	2055.9	$1.49\cdot10^{-10}$
Copper foam II	85	$2.0\cdot10^{-4}$	1233.5	$1.82\cdot10^{-9}$
Groove I	18	$2.31\cdot10^{-4}$	1068.0	$5.07\cdot10^{-10}$
Groove II	21	$3.33\cdot10^{-4}$	740.9	$2.35\cdot10^{-9}$

counts for excellent heat transfer performance of copper foam-type 1 in spite of its low permeability. Therefore, it infers that the capillary pressure is a more important factor for performance. This is also evidenced by both grooved-type cases. Because of the smaller channel hydraulic diameter, the larger capillary pressure could drive enough condensation liquid back to evaporation region, which improves the performance of the grooved-type VC. The thermal resistance of the grooved-type II, with the maximum channel number, is unexpectedly large though having large permeability. It may be related to its low water-charging rate. The influence of charging rate needs further research.

Spread thermal resistance

The heat diffusion performances of tested samples were also explored. The spread thermal resistance is defined as the temperature difference between the center point of bottom surface and the corner point of upper surface. It follows Reay *et al.* [15]:

$$R = \frac{T_h - T_a}{Q} \tag{2}$$

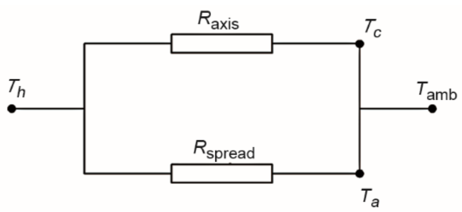

Figure 8. Thermal resistance network of VC

where T_h is the center temperature of the bottom surface, T_a – the corner temperature of the condensation surface, and Q – the input heating power.

The thermal resistance network is illustrated in fig. 8. It is mainly composed of axis and spread thermal resistance in a parallel relationship. Different from heat pipe, the heat diffusion effect is of great importance for VC. The heat diffusion performance could be weighed by the spread thermal resistance [15].

For the upper surface of VC, the temperature at the center point is generally higher than those at the corner points. The spread thermal resistance of grooved-type samples is plotted against heat power in fig. 9 and that of the copper foam-type ones in fig. 10. The grooved samples shows lower spread thermal resistance than the copper foam ones in the same heating power. It indicates that the grooved wick facilities temperature uniformity. Interestingly, the grooved-type 1 presents the lowest heat spread resistance of all samples, but not guarantees the lowest axis thermal resistance. It is speculated that the radial distribution of micro-grooves accounts for its excellent temperature uniformity. The radial design is helpful for the heat diffusion performance along the evaporation surface. By contrast, the copper foam-type I is not superior in heat diffusion performance, but has the lowest axis thermal resistance of all samples. In terms of thermal resistance network, overall thermal resistance of VC is composed of the axis thermal resistance and spread thermal resistance in parallel. The overall performance of VC is determined mutually by both axis and spread thermal resistance. There is a wax and wane relationship between the two.

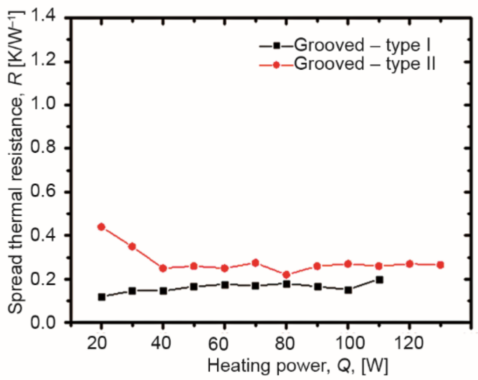

Figure 9. Spread thermal resistance of grooved-type VC

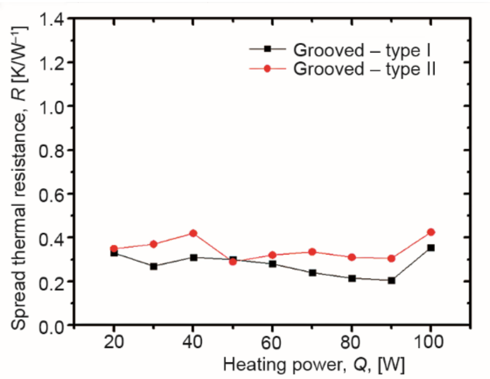

Figure 10. Spread thermal resistance of copper foam-type VC

Visual observation

The internal evaporation process in the copper foam-type I was examined at different water-charging rate. The heater area is 9 cm^2. It was first conducted on the case of the 30% charging rate. The observation results are shown in fig. 11 at q = 7 W/cm^2. In the center region of the evaporation surface, the dry-out phenomenon was clearly observed. With the increase of heat flux, the boundary line of drying out region moves outwards and the original wet area becomes dry. As the heat flux reaches 12 W/cm^2, the speed of drying out becomes faster. The pool boiling process is not observed instead of a typical thin film evaporation phenomenon. Then, the case of 100% liquid-charging rate is further on. If the heat flux is less than 8 W/cm^2, the evaporation surface is dominated by the thin film evaporation mechanism. But after $q \geq 8$ W/cm^2, the result is shown in fig. 12. The white spots represent the reflection of water droplets to the incident LED light, the black ones represent the pores of the wick structure, and the gray ones mean the skeleton of the structure. Intermittent flash occurred in a specified white pore region with a cycle period 0.026 seconds in operation. The high-speed photography system takes pictures at a speed of 500 times per second. The liquid level fluctuation in the pore region infers the pool boiling mode in the evaporation surface. The rise and fall of the liquid level is caused by the expansion and rupture of bubbles in the porous structure.

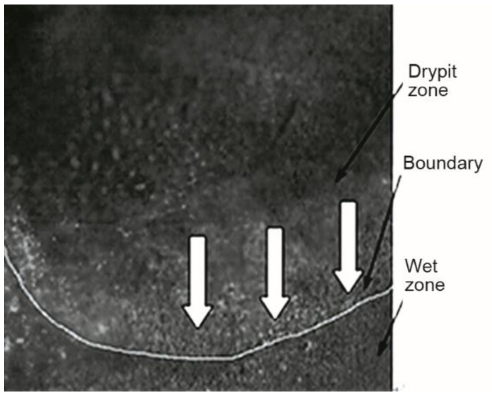

Figure 11. Dry-out area of evaporating surface

For the grooved-type I sample with a charging rate of 100%, the internal process was also studied. The heater area is 2.25 cm^2. While the input heating power was 10 W/cm^2, the condensate was found to be sucked into the channel and accumulated in the center of evaporation surface. And up to 30 W/cm^2, some bubbles were generated continuously and the pool boiling process was dominated. At $q \geq 40$ W/cm^2, bubbles were produced at a very rapid rate, fig. 13. At the same time, the condensing rate around the acrylic plate also becomes very fast. A vigorous pool boiling phenomenon occurred in the evaporation surface.

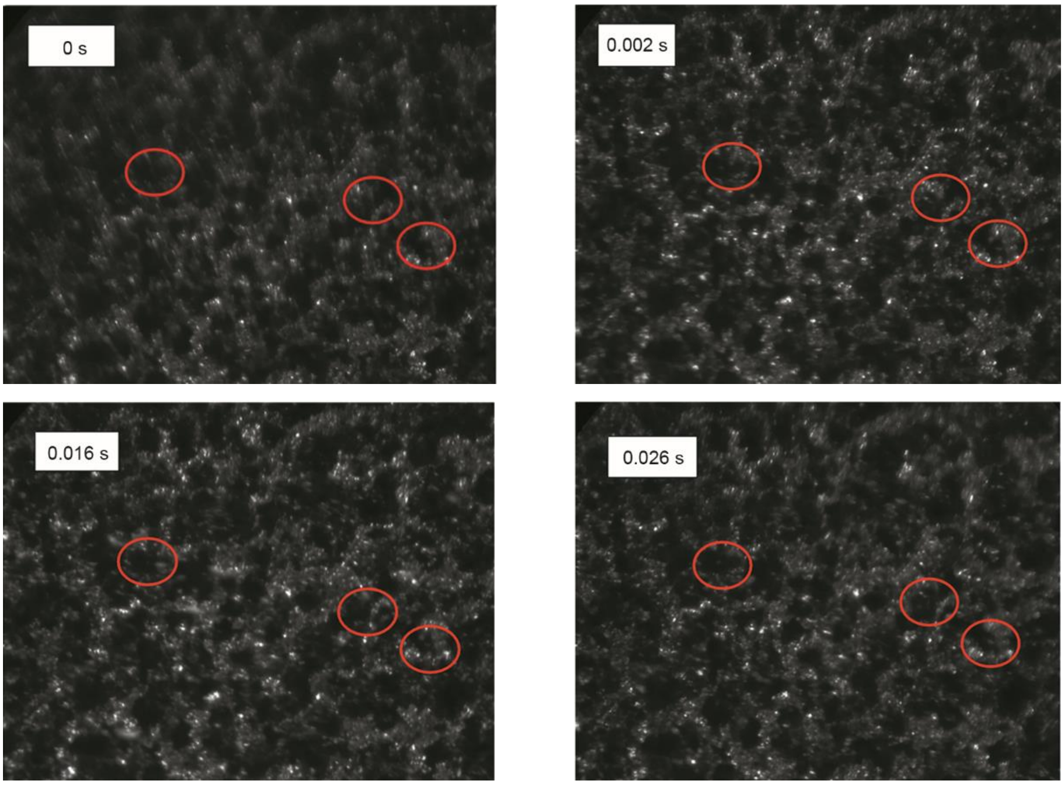

Figure 12. Pulsed boiling process of the copper foam VC

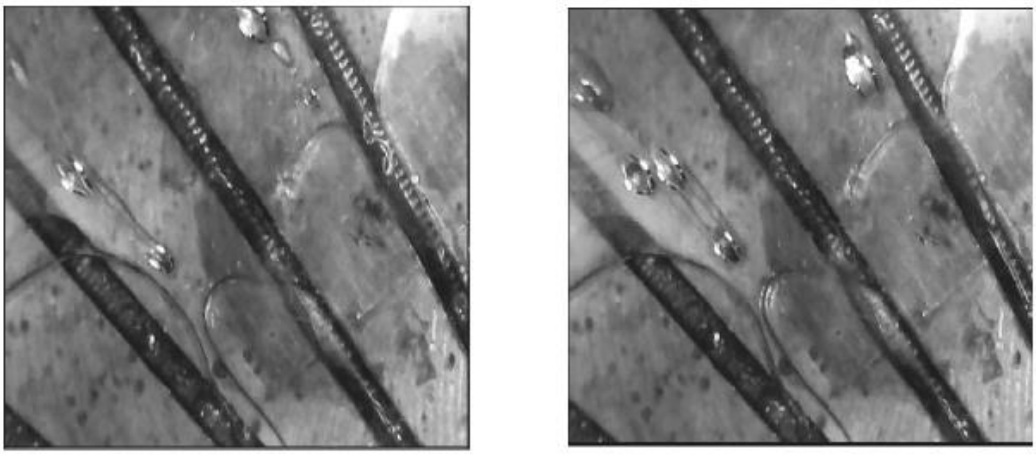

Figure 13. Boiling process of grooved VC

Conclusions

Both kinds of VC were extensively investigated in this study. Key findings from present study are summarized as follows.

- The copper foam-type VC presents slightly lower in thermal resistance than the grooved-type ones. The axis resistance of VC is mainly affected by the permeability, capillary pressure and charging rate. Maximum capillary force accounts for excellent heat transfer performance of copper foam-type I in spite of its low permeability.
- The grooved-type I presented the lowest heat spread resistance of all samples, but not guaranteed the lowest axis thermal resistance. The copper foam-type I is not superior in heat diffusion ability, but has the lowest axis thermal resistance of all samples. There is a wax and wane relationship between both kinds of resistances.
- For the copper-foam VC, the evaporation surface is mainly dominated by the thin film evaporation mechanism at low charging rate while it transformed to the pool boiling mechanism at high charging rate. For the grooved VC, the heat transfer process on the evaporation surface is mainly dominated by the pool boiling mechanism regardless of the charging rate.

This study would pave the ways for further understanding the operating mechanism of thinner VC.

Acknowledgment

We gratefully acknowledge the financial support of and the Jiangsu University of Science and Technology Foundation (35011001).

References

[1] Mizuta, K., *et al.*, Development and Characterization of a Flat Laminate Vapor Chamber, *Applied Thermal Engineering*, *104* (2016), July, pp. 461‑471
[2] Justin, A., *et al.*, Recent Advances in Vapor Chamber Transport Characterization for High-Heat-Flux Applications, *Advances in Heat Transfer*, *45* (2013), Dec., pp. 209-290
[3] Boukhanouf, R., Haddad, A., Experimental Investigation of a Flat Plate Heat Pipe Performance Using IR Thermal Imaging, *Applied Thermal Engineering*, *26* (2006), 17-18, pp. 2148-2156
[4] Lefevre, F., *et al*., Flat Plate Heat Pipes: From Observations to the Modeling of the Capillary Structure, *Frontiers in Heat Pipes*, *3* (2012), 1, pp. 1-6
[5] Hwang, G. S., *et al*., Multi-Artery Heat Pipe Spreader: Experiment, *International Journal of Heat and Mass Transfer*, *53* (2010), 13-14, pp. 2662-2669
[6] Guangmeng, Z., *et al.*, A Visualization Study of the Influences of Liquid Levels on Boiling and Condensation Co-Existing Phase Change Heat Transfer Phenomenon in Small Confined Spaces, *International Journal of Heat and Mass Transfer*, *73* (2014), June, pp. 415-423
[7] Xianbing, J., *et al.*, Copper Foam Based Vapor Chamber for High Heat Flux Dissipation, *Experimental thermal and fluid Science*, *40* (2012), July, pp. 93-102
[8] Wong, S. C., *et al.*, Visualization and Evaporator Resistance Measurement in Heat Pipes Charged with Water, Methanol or Acetone, *International Journal of Thermal Sciences*, *52* (2012), Feb., pp. 154-160
[9] Chen, Y.-T., *et al.*, Feasibility Study of an Aluminum Vapor Chamber with Radial Grooved and Sintered Powders Wick Structures, *Applied Thermal Engineering*, *51* (2013), 1-2, pp. 864-870
[10] Weibel, J. A., Garimella, S. V., Visualization of Vapor Formation Regimes During Capillary-Fed Boiling in Sintered-Powder Heat Pipe Wicks, *International Journal of Heat and Mass Transfer*, *55* (2012), 13-14, pp. 3498‑3510
[11] Zhaoshu, C., *et al.*, Design Fabrication and Thermal Performance of a Novel Ultra-Thin Vapour Chamber for Cooling Electronic Devices, *Energy Conversion & Management*, *187* (2019), May, pp. 221-231
[12] Srivathsan, S., *et al.*, The Role of Vapor Venting and Liquid Feeding on the Dry-Out Limit of evaporator Two-Layer wicks, *International Journal of Heat and Mass Transfer*, *148* (2020), Feb., 119063

[13] Rongfu, W., *et al.*, Capillary-Driven Liquid Film Boiling Heat Transfer on Hybrid Mesh Wicking Structures, *Nano Energy*, *51* (2018), Sept., pp. 373-382
[14] Xianbing, J., *et al.*, Switchable Heat Transfer Mechanisms of Nucleation and Convection By wettability Match of Evaporator and Condenser for Heat Pipes: Nanostructured surface Effect, *Nano Energy*, *38* (2017), Aug., pp. 313-325
[15] Reay, D. A., *et al.*, *Heat Pipes: Theory, Design and Applications,* 6th ed., Elsevier Science & Technology, Amsterdam, The Netherlands, 2014

Paper submitted: August 21, 2020
Paper revised: December 15, 2020
Paper accepted: December 20, 2020